

Article

Highly Efficient Numerical Integrator for the Circular Restricted Three-Body Problem

Xiongbiao Tu ^{1,*} , Qiao Wang ^{1,2} and Yifa Tang ^{3,4}

¹ National Astronomical Observatories, Chinese Academy of Sciences, Beijing 100101, China

² School of Astronomy and Space Science, University of Chinese Academy of Sciences, Beijing 100049, China

³ LSEC, ICMSEC, Academy of Mathematics and Systems Science, Chinese Academy of Sciences, Beijing 100190, China

⁴ School of Mathematical Sciences, University of Chinese Academy of Sciences, Beijing 100049, China

* Correspondence: tuxb@nao.cas.cn

Abstract: The dynamic equation of a mass point in the circular restricted three-body problem is governed by Coriolis and centrifugal force, in addition to a co-rotating potential relative to the frame. In this paper, we provide an explicit, symmetric integrator for this problem. Such an integrator is more efficient than the symplectic Euler method and the Gauss Runge–Kutta method as regards this problem. In addition, we proved the integrator is symplectic by the discrete Hamilton’s principle. Several groups of numerical experiments demonstrated the precision and high efficiency of the integrator in the examples of the quadratic potential and the bounded orbits in the circular restricted three-body problem.

Keywords: high efficiency; symplectic; restricted three-body



Citation: Tu, X.; Wang, Q.; Tang, Y. Highly Efficient Numerical Integrator for the Circular Restricted Three-Body Problem. *Symmetry* **2022**, *14*, 1769. <https://doi.org/10.3390/sym14091769>

Academic Editor: Jan Awrejcewicz

Received: 18 July 2022

Accepted: 22 August 2022

Published: 25 August 2022

Publisher’s Note: MDPI stays neutral with regard to jurisdictional claims in published maps and institutional affiliations.



Copyright: © 2022 by the authors. Licensee MDPI, Basel, Switzerland. This article is an open access article distributed under the terms and conditions of the Creative Commons Attribution (CC BY) license (<https://creativecommons.org/licenses/by/4.0/>).

1. Introduction

As space science advances, spacecraft orbit design missions become more complex, and as a result the need for advanced and efficient algorithms has grown. For example, the recently launched James Webb Space Telescope orbits the Halo orbit (Figure 1) near the second Lagrangian point L_2 of the Sun-Earth restricted three-body problem. Since this Halo orbit is chaotic, the telescope needs to recalibrate the orbit after a timescale. The circular restricted three-body problem is a non-canonical Hamiltonian system, which can be transformed into canonical form. Explicit symplectic algorithms such as the symplectic Euler method can be used to the canonical form, but we argue below that our proposed method is more efficient. This paper provides a highly efficient algorithm for numerical orbit design and recalibration of orbits to the circular restricted three-body problem.

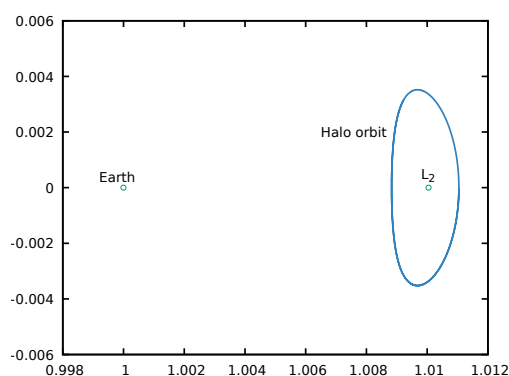


Figure 1. Halo orbit nearby the collinear libration point L_2 of Sun-Earth system. The James Webb Space Telescope is located in this Halo orbit.

The canonical Hamiltonian system could be the most important physical systems and a canonical Hamiltonian system in the variables $\mathbf{z} = (p, q)$ given in the form

$$\begin{aligned}\dot{p} &= -H_q(p, q) \\ \dot{q} &= H_p(p, q)\end{aligned}\quad (1)$$

where $p, q \in \mathbb{R}^d$. Or equivalently

$$\dot{\mathbf{z}} = J^{-1} \nabla H(\mathbf{z}), \quad J = \begin{pmatrix} 0 & I_d \\ -I_d & 0 \end{pmatrix}, \quad (2)$$

where I_d is a $d \times d$ identity matrix. It has an outstanding property that the flow of Hamiltonian system is symplectic. It naturally finds those discrete systems that preserve the properties of symplecticity and the inner symmetries of original Hamiltonian system. Therefore, the symmetric, symplectic algorithms [1–5] are the standard methods to such problems. In addition, efficient structure-preserving methods [6,7] are also a research focus.

The well-known Boris algorithm [8–13] in the plasma dynamics has some good geometric properties. Generally, it is symmetric, second-order, volume-preserving [9], and not symplectic [10]. However, in special configuration of the homogeneous magnetic field, the integrator is variational symplectic and preserves near-conservation of energy over long-term evolution [10,14].

This paper is organized as follows. In Section 2, we gave a brief introduction to co-rotating coordinate systems and the proposed explicitly symmetric integrator ψ_b . In Sections 3 and 4, we analyzed long term energy behaviors for this integrator and proved its symplectic property. In Section 5, two groups of numerical experiments were conducted to check the precision and high efficiency of the integrator. Finally, we summarize this work in Section 6.

2. Numerical Methods

2.1. The Co-rotating System

The circular restricted three-body problem [15,16] is a kind of co-rotating system, which can be written as

$$\ddot{\mathbf{x}} + 2(\boldsymbol{\Omega} \times \dot{\mathbf{x}}) = -\nabla(U(\mathbf{x}) - \frac{1}{2}\omega^2 \mathbf{r}^2), \quad (3)$$

where $\mathbf{x} = (x, y, z)$ is the position, $\boldsymbol{\Omega} = (0, 0, \omega)$ means the system rotates clockwise around the z axis with rotation speed ω , $U(\mathbf{x})$ is a potential energy, and $\mathbf{r} = (x, y, 0)$. It is a Euler–Lagrange equation with Lagrangian $L(\mathbf{x}, \dot{\mathbf{x}}) = \frac{1}{2}\dot{\mathbf{x}}^2 + \boldsymbol{\Omega} \cdot (\mathbf{r} \times \dot{\mathbf{r}}) - (U(\mathbf{x}) - \frac{1}{2}\omega^2 \mathbf{r}^2)$, the conjugate momenta $\mathbf{p} = \partial L / \partial \dot{\mathbf{x}} = \dot{\mathbf{x}} + (-\omega y, \omega x, 0) \triangleq \dot{\mathbf{x}} + \mathbf{A}(\mathbf{x})$ (conjugate to the position variables \mathbf{x}) derived by Legendre transform. The energy $E = \frac{1}{2}\dot{\mathbf{x}}^2 + (U(\mathbf{x}) - \frac{1}{2}\omega^2 \mathbf{r}^2)$ is an invariant along the flow of the system. It is special that different physical processes imply similar physical laws. For the charged particle in the electromagnetic field, its dynamics are governed by the Newton–Lorentz equation, which has a similar form to Equation (3). In particular, $\boldsymbol{\Omega}$ plays the role of the magnetic field, $U(\mathbf{x}) - \frac{1}{2}\omega^2 \mathbf{r}^2$ acts as the scalar potential.

We set $\varphi(\mathbf{x}) = U(\mathbf{x}) - \frac{1}{2}\omega^2 \mathbf{r}^2$ and rewrite the co-rotating coordinate system (3) in the form of $\mathbf{z} = (\mathbf{x}, \mathbf{p})$. The motion equations of the mass point can be expressed as

$$\begin{cases} \dot{\mathbf{x}} = H_{\mathbf{p}}(\mathbf{z}) = \mathbf{p} - \mathbf{A}(\mathbf{x}), \\ \dot{\mathbf{p}} = -H_{\mathbf{x}}(\mathbf{z}) = \left(\frac{\partial \mathbf{A}(\mathbf{x})}{\partial \mathbf{x}} \right)^{\top} (\mathbf{p} - \mathbf{A}(\mathbf{x})) - \nabla \varphi(\mathbf{x}), \end{cases} \quad (4)$$

where $H(\mathbf{z}) = \frac{1}{2}(\mathbf{p} - \mathbf{A}(\mathbf{x}))^2 + \varphi(\mathbf{x})$. Obviously, it is a canonical Hamiltonian system $\dot{\mathbf{z}} = J^{-1} \nabla H(\mathbf{z})$ with

$$J = \begin{pmatrix} 0 & -I_3 \\ I_3 & 0 \end{pmatrix}.$$

The antisymmetric matrix J provides a symplectic structure, which is defined by

$$w_J = \frac{1}{2} dz^\top \wedge J dz.$$

An integrator $\psi : \mathbf{z}_n \mapsto \mathbf{z}_{n+1}$ is called symplectic, when w_J is preserved by the flow of the integrator, i.e., $dz_{n+1}^\top \wedge J dz_{n+1} = dz_n^\top \wedge J dz_n$.

2.2. The Explicitly Symmetric Integrator ψ_b

First, we take into account the Boris algorithm [8–13] to make discrete the system (3) as the numerical integrator ψ_b :

$$\frac{\mathbf{x}_{n+1} - 2\mathbf{x}_n + \mathbf{x}_{n-1}}{\Delta t^2} + 2\Omega \times \frac{\mathbf{x}_{n+1} - \mathbf{x}_{n-1}}{2\Delta t} = -\nabla\varphi(\mathbf{x}_n). \tag{5}$$

The scheme is a second-order explicitly symmetric integrator. At the same time, we set the conjugate momenta to be the form of

$$\begin{aligned} \mathbf{p}_n &= \frac{\mathbf{x}_{n+1} - \mathbf{x}_n}{\Delta t} - (\mathbf{x}_{n+1} - \mathbf{x}_n) \times \Omega + \mathbf{A}(\mathbf{x}_n) + \Delta t \nabla\varphi(\mathbf{x}_n), \\ \mathbf{p}_{n+1} &= \frac{\mathbf{x}_{n+1} - \mathbf{x}_n}{\Delta t} + (\mathbf{x}_{n+1} - \mathbf{x}_n) \times \Omega + \mathbf{A}(\mathbf{x}_{n+1}). \end{aligned} \tag{6}$$

The map $(\mathbf{x}_n, \mathbf{p}_n) \mapsto (\mathbf{x}_{n+1}, \mathbf{p}_{n+1})$ is symplectic which will be verified in Section 4.

In the following sections, we analyze the energy errors over long times and the symplectic property of the numerical integrator ψ_b .

3. Energy Error Analysis

In this section, we analyze the energy deviation of the integrators ψ_b over very long times. First, we consider ψ_b and solve the modified differential equation whose solution $\mathbf{y}(t)$ formally satisfies $\mathbf{y}(n\Delta t) = \mathbf{x}_n$. Thus, $\mathbf{y}(t)$ must satisfy Equation (5), i.e.,

$$\begin{aligned} &\frac{\mathbf{y}(t + \Delta t) - 2\mathbf{y}(t) + \mathbf{y}(t - \Delta t)}{\Delta t^2} + \\ &2\Omega \times \frac{\mathbf{y}(t + \Delta t) - \mathbf{y}(t - \Delta t)}{2\Delta t} = -\nabla\varphi(\mathbf{y}(t)). \end{aligned} \tag{7}$$

We expand all terms into powers of Δt at the time t then obtain the following modified differential equation

$$\begin{aligned} &(\ddot{\mathbf{y}} + \frac{\Delta t^2}{12}\mathbf{y}^{(4)} + \dots) + \\ &\Omega \times (2\dot{\mathbf{y}} + \frac{\Delta t^2}{3}\mathbf{y}^{(3)} + \dots) = -\nabla\varphi(\mathbf{y}). \end{aligned} \tag{8}$$

Multiplying $\dot{\mathbf{y}}^\top$ in the two sides of the formula. Since $\dot{\mathbf{y}}^\top (\Omega \times \dot{\mathbf{y}}) = 0$, we derive

$$\begin{aligned} &\dot{\mathbf{y}}^\top (\ddot{\mathbf{y}} + \frac{\Delta t^2}{12}\mathbf{y}^{(4)} + \dots) + \\ &\dot{\mathbf{y}}^\top \Omega \times (\frac{\Delta t^2}{3}\mathbf{y}^{(3)} + \dots) = -\dot{\mathbf{y}}^\top \nabla\varphi(\mathbf{y}). \end{aligned} \tag{9}$$

The left-hand side can be written as the full differential and $\dot{\mathbf{y}}^\top \nabla\varphi(\mathbf{y}(t)) = \frac{d}{dt}\varphi(\mathbf{y}(t))$, so the modified differential equation has a formal invariant, i.e.,

$$\begin{aligned} &\frac{d}{dt} \left(\frac{1}{2}\dot{\mathbf{y}}^\top \dot{\mathbf{y}} + \varphi(\mathbf{y}) + \frac{\Delta t^2}{12}(\dot{\mathbf{y}}^\top \mathbf{y}^{(3)} - \frac{1}{2}\dot{\mathbf{y}}^\top \ddot{\mathbf{y}} \right. \\ &\left. + 4\dot{\mathbf{y}}^\top (\Omega \times \dot{\mathbf{y}}) + \dots \right) = 0. \end{aligned} \tag{10}$$

Thus, we obtain a new formal generalized energy $E_h(\mathbf{y}, \dot{\mathbf{y}}) = E(\mathbf{y}, \dot{\mathbf{y}}) + \Delta t^2 E_2(\mathbf{y}, \dot{\mathbf{y}}) + \dots$, which is an invariant. We only consider the numerical integrator $\{(\mathbf{x}_n, \dot{\mathbf{x}}_n)\}$ in a

compact set D . To estimate the energy error of the integrator ψ_b over a long time, we truncate the E_h in N leading terms, and integrate over the time interval $[0, n\Delta t]$,

$$E_h^N(\mathbf{x}_n, \dot{\mathbf{x}}_n) - E_h^N(\mathbf{x}_0, \dot{\mathbf{x}}_0) = n\Delta t \mathcal{O}(\Delta t^N). \quad (11)$$

The right-hand side in Formula (11) is a high order infinitesimal quantity, so

$$|E(\mathbf{x}_n, \dot{\mathbf{x}}_n) - E(\mathbf{x}_0, \dot{\mathbf{x}}_0)| \leq C_N \Delta t^2. \quad (12)$$

where C_N is directly dependent on the values of $\dot{\mathbf{y}}^\top \mathbf{y}^{(3)} - \frac{1}{2} \dot{\mathbf{y}}^\top \ddot{\mathbf{y}} + 4\dot{\mathbf{y}}^\top (\Omega \times \ddot{\mathbf{y}})$ in the compact set D .

4. The Symplectic Property

In canonical Hamiltonian system, a map $\phi : \mathbf{z}_n \mapsto \mathbf{z}_{n+1}$, $\mathbf{z} \in \mathbb{R}^{2d}$ is called symplectic if its Jacobian matrix satisfies the symplectic condition,

$$\left(\frac{\partial \phi}{\partial \mathbf{z}_n} \right)^\top J \left(\frac{\partial \phi}{\partial \mathbf{z}_n} \right) = J. \quad (13)$$

The equivalent form is that the map ϕ preserves a standard symplectic structure $\frac{1}{2} d\mathbf{z}^\top \wedge J d\mathbf{z}$, i.e., $d\mathbf{z}_{n+1}^\top \wedge J d\mathbf{z}_{n+1} = d\mathbf{z}_n^\top \wedge J d\mathbf{z}_n$.

In this subsection, we show that the numerical integrator ψ_b is symplectic. We choose the discrete Lagrangian L_h as

$$L_h(\mathbf{x}_n, \mathbf{x}_{n+1}) = \frac{1}{2\Delta t} (\mathbf{x}_{n+1} - \mathbf{x}_n)^2 + \frac{1}{2} \Omega \cdot (\mathbf{r}_n + \mathbf{r}_{n+1}) \times (\mathbf{r}_{n+1} - \mathbf{r}_n) - \Delta t \varphi(\mathbf{x}_n). \quad (14)$$

The discrete form of $\int_{t_0}^{t_N} L(\mathbf{x}(t), \dot{\mathbf{x}}(t)) dt$, i.e., the action S_h is

$$S_h(\mathbf{x}_0, \dots, \mathbf{x}_N) = \sum_{n=0}^{N-1} L_h(\mathbf{x}_n, \mathbf{x}_{n+1}), \quad (15)$$

where L_h is the discrete Lagrangian. According to the discrete Hamilton's principle, the discrete Euler–Lagrange equation reads

$$D_2 L_h(\mathbf{x}_{n-1}, \mathbf{x}_n) + D_1 L_h(\mathbf{x}_n, \mathbf{x}_{n+1}) = 0, \quad (16)$$

$$\begin{aligned} \mathbf{p}_n &= -D_1 L_h(\mathbf{x}_n, \mathbf{x}_{n+1}), \\ \mathbf{p}_{n+1} &= D_2 L_h(\mathbf{x}_n, \mathbf{x}_{n+1}), \end{aligned} \quad (17)$$

where D_i is the partial derivative with respect to the i -th argument. The corresponding formula of the formulation (17) is the formula (6). By eliminating \mathbf{p}_n , the evolution formulation of \mathbf{x}_n can be obtained, which is ψ_b , as follows

$$\frac{\mathbf{x}_{n+1} - 2\mathbf{x}_n + \mathbf{x}_{n-1}}{\Delta t} + 2\Omega \times \frac{\mathbf{x}_{n+1} - \mathbf{x}_{n-1}}{2} = -\Delta t \nabla \varphi(\mathbf{x}_n). \quad (18)$$

A straightforward calculation gives the equation of $d\mathbf{p}_{n+1} \wedge d\mathbf{x}_{n+1} = d\mathbf{p}_n \wedge d\mathbf{x}_n$ (refer to the Theorem 5.1 of Chapter 6 in Hairer [17]). It proves that the integrator ψ_b is symplectic and defines a symplectic map $(\mathbf{p}_n, \mathbf{x}_n) \mapsto (\mathbf{p}_{n+1}, \mathbf{x}_{n+1})$.

It is also well-known that the symplectic integrator has the property of near-conservation of energy over a long time. The error expression (12) is estimated by taking into account the formal energy of the modified equation [18].

5. Numerical Experiments

In this section, we numerically present the behaviors of the integrator ψ_b in two kinds of potential energy, an extensive Quadratic potential and restricted three-body Earth-Moon

system. At the same time, we compare our results with those of the well-known symplectic Euler method ψ_{sE} and the highly efficient Gauss Runge–Kutta method in the canonical form (4).

In the case of the canonical system, we make discrete the system (4) by the symplectic Euler method ψ_{sE} :

$$(a) : \begin{cases} \mathbf{x}_{n+\frac{1}{2}} = \mathbf{x}_n + \Delta t H_{\mathbf{p}}(\mathbf{x}_n, \mathbf{p}_{n+\frac{1}{2}}) \\ \mathbf{p}_{n+\frac{1}{2}} = \mathbf{p}_n - \Delta t H_{\mathbf{x}}(\mathbf{x}_n, \mathbf{p}_{n+\frac{1}{2}}), \end{cases} \tag{19}$$

and

$$(b) : \begin{cases} \mathbf{x}_{n+1} = \mathbf{x}_{n+\frac{1}{2}} + \Delta t H_{\mathbf{p}}(\mathbf{x}_{n+1}, \mathbf{p}_{n+\frac{1}{2}}) \\ \mathbf{p}_{n+1} = \mathbf{p}_{n+\frac{1}{2}} - \Delta t H_{\mathbf{x}}(\mathbf{x}_{n+1}, \mathbf{p}_{n+\frac{1}{2}}). \end{cases} \tag{20}$$

This numerical integrator ψ_{sE} is a 2nd order explicitly symmetric symplectic numerical integrator for the canonical system (4). The explicit form of ψ_{sE} reads

$$(a) : \begin{cases} \mathbf{x}_{n+\frac{1}{2}} = D\mathbf{x}_n + \Delta t \mathbf{p}_{n+\frac{1}{2}} \\ \mathbf{p}_{n+\frac{1}{2}} = T(\mathbf{p}_n - \Delta t \nabla U(\mathbf{x}_n)), \end{cases} \tag{21}$$

and

$$(b) : \begin{cases} \mathbf{x}_{n+1} = T(\mathbf{x}_{n+\frac{1}{2}} + \Delta t \mathbf{p}_{n+\frac{1}{2}}) \\ \mathbf{p}_{n+1} = D\mathbf{p}_{n+\frac{1}{2}} - \Delta t \nabla U(\mathbf{x}_{n+1}). \end{cases} \tag{22}$$

In here, the matrices T and D are as follows

$$T = \begin{pmatrix} \frac{1}{1+(\Delta t\omega)^2} & \frac{\Delta t\omega}{1+(\Delta t\omega)^2} & 0 \\ \frac{-\Delta t\omega}{1+(\Delta t\omega)^2} & \frac{1}{1+(\Delta t\omega)^2} & 0 \\ 0 & 0 & 1 \end{pmatrix}, \quad D = \begin{pmatrix} 1 & \Delta t\omega & 0 \\ -\Delta t\omega & 1 & 0 \\ 0 & 0 & 1 \end{pmatrix}.$$

In addition, the 2nd order symmetric symplectic integrator ψ_b is explicit, as follows

$$\mathbf{x}_{n+1} = T(2\mathbf{x}_n - D\mathbf{x}_{n-1} - \Delta t^2 \nabla \varphi(\mathbf{x}_n)). \tag{23}$$

5.1. Quadratic Potential

We consider a homogeneous rotating top-hat density sphere with the quadratic potential of $U(\mathbf{x}) = 4(x^2 + y^2 + z^2)$. We set the rotating speed $\omega = \pi/40$ and the period is 80. The initial position and velocity are $\mathbf{x} = (-1.9, 0, 0)$ and $\mathbf{v} = (0, -2.0, 0)$, respectively.

We integrate the initial value problem in a time interval $[0, T]$ with $T = 8 \times 10^4$ with different step-sizes $\Delta t = T/n$. We denote the maximum energy variation by

$$\text{err}_H(T/n) = \max_{k=1, \dots, n} \left| \frac{H(\mathbf{z}^k) - H(\mathbf{z}^0)}{H(\mathbf{z}^0)} \right|. \tag{24}$$

In Figure 2, we observe that the numerical integrators ψ_b, ψ_{sE} both give the accurate orbit in the first rotation period and the 1000th rotation period. The work efficiency diagram of maximum energy variation along the trajectory versus the CPU time (in seconds) is displayed in Figure 3, both on the logarithmic scale. We observe that our integrator ψ_b is more efficient than the integrator ψ_{sE} . In actually, with the same maximum energy variation, the efficiency of ψ_b is increased by about 40% versus ψ_{sE} .

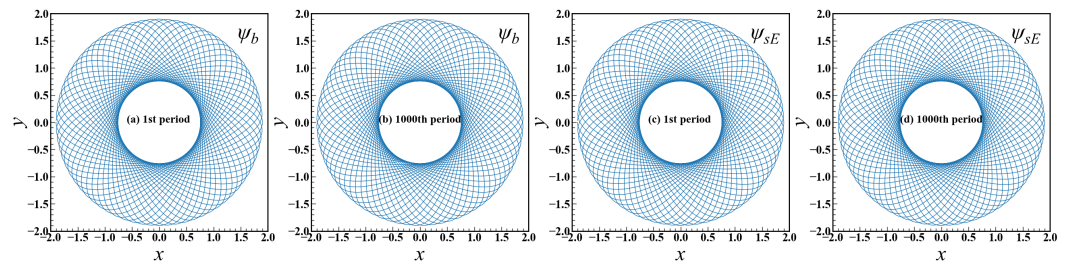


Figure 2. The orbits are given by ψ_b and ψ_{sE} in the first rotation period (a,c) and the 1000th rotation period (b,d).

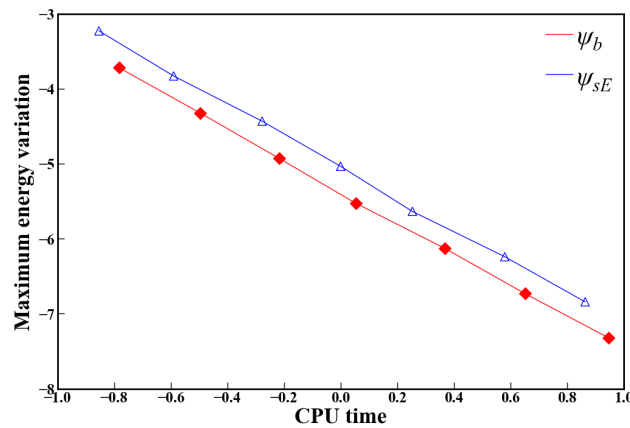


Figure 3. Maximum energy variation $err_H(\Delta t)$ versus the CPU time in double logarithmic scale, which are given by ψ_b and ψ_{sE} over the time interval $[0, T]$.

5.2. Earth-Moon System

In the design of a spacecraft’s orbit, the earth and moon’s disturbances should be taken into account, and the spacecraft can be seen as a mass point. In this case, the motions of the earth, moon, and satellite form a circular restricted three-body problem. The circular restricted three-body problem can be written in the form of (3) with potential

$$U(\mathbf{x}) = - \frac{GM_1}{\sqrt{(x - x_1)^2 + (y - y_1)^2 + z^2}} - \frac{GM_2}{\sqrt{(x - x_2)^2 + (y - y_2)^2 + z^2}}, \tag{25}$$

which has been widely studied [15,16,19–21]. We expand into the component form of (x, y, z) , as follow

$$\begin{aligned} \frac{d^2x}{dt^2} - x\omega^2 - 2\omega \frac{dy}{dt} &= - \frac{GM_1(x - x_1)}{R_1^3} - \frac{GM_2(x - x_2)}{R_2^3}, \\ \frac{d^2y}{dt^2} - y\omega^2 + 2\omega \frac{dx}{dt} &= - \frac{GM_1(y - y_1)}{R_1^3} - \frac{GM_2(y - y_2)}{R_2^3}, \\ \frac{d^2z}{dt^2} &= - \frac{GM_1z}{R_1^3} - \frac{GM_2z}{R_2^3}, \end{aligned}$$

where $R_1 = ((x - x_1)^2 + (y - y_1)^2 + z^2)^{1/2}$, $R_2 = ((x - x_2)^2 + (y - y_2)^2 + z^2)^{1/2}$ and the coordinate origin is mass center of the system.

In this example of an Earth-Moon system, the unit of distance is an Astronomical Unit (1.4959787×10^{13} cm), the time unit is an earth day (86,400 s), and the mass unit is in kilograms. The corresponding normalized parameters $GM_1 = 0.8997011603631609 \times 10^{-9}$ (following the parameters in [22]), $GM_2 = 0.0123 GM_1$, the distance of between earth

and moon $R = 2.56267 \times 10^{-3}$, $r_1 = -M_2R/(M_1 + M_2) = -3.113784550034574 \times 10^{-5}$, $r_2 = M_1R/(M_1 + M_2) = 2.53153215449654 \times 10^{-3}$ and the rotation speed $\omega = \sqrt{G(M_1 + M_2)/R^3}$. The earth position is $(x_1, y_1) = (r_1, 0)$ and the moon position is $(x_2, y_2) = (r_2, 0)$. We set two groups of initial conditions to check the behaviors of the numerical integrators ψ_b and ψ_{sE} .

Orbit 1: we set initial position of the mass point at $\mathbf{x} = (-r_2/4, 0, 0)$, velocity $\dot{\mathbf{x}} = (0, 1.69561 \times 10^{-3}, 0)$. The orbit of the mass point is numerically integrated over a time interval $[0, 4 \times 10^4]$.

Orbit 2: we set initial position of the mass point at $\mathbf{x} = (-3r_2/5, 0, 0)$, velocity $\dot{\mathbf{x}} = (0, 1.35057 \times 10^{-3}, 0)$. The orbit is integrated over a time interval $[0, 10^5]$.

We integrate the initial value problem with different step-sizes $\Delta t = T/n$. Following the numerical experiment 1, the maximum energy variation is as follows

$$\text{err}_H(T/n) = \max_{k=1, \dots, n} \left| \frac{H(\mathbf{z}^k) - H(\mathbf{z}^0)}{H(\mathbf{z}^0)} \right|. \tag{26}$$

Figure 4 shows that for different initial values, the numerical integrators ψ_b, ψ_{sE} both give the accurate orbit over a long time. Figure 5 shows that the work efficiency diagram of maximum energy variation along the trajectory versus the CPU time (in seconds) in double logarithmic scale with the initial values of orbit 1 and orbit 2. We conclude that our integrator ψ_b is more efficient than the integrator ψ_{sE} .

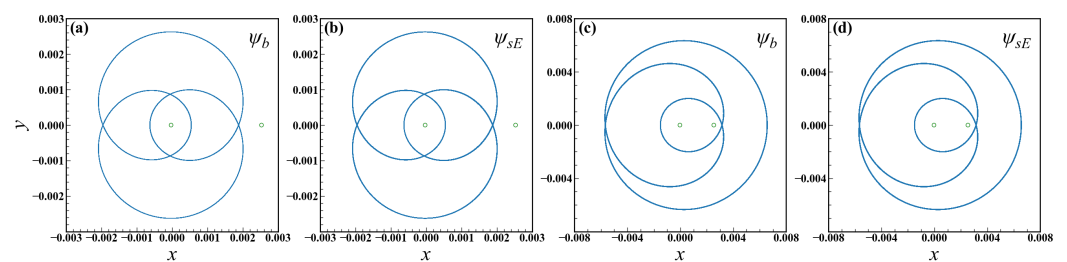


Figure 4. Numerical orbits are given by ψ_b, ψ_{sE} with the initial values of orbit 1 (a,b) and orbit 2 (c,d), respectively.

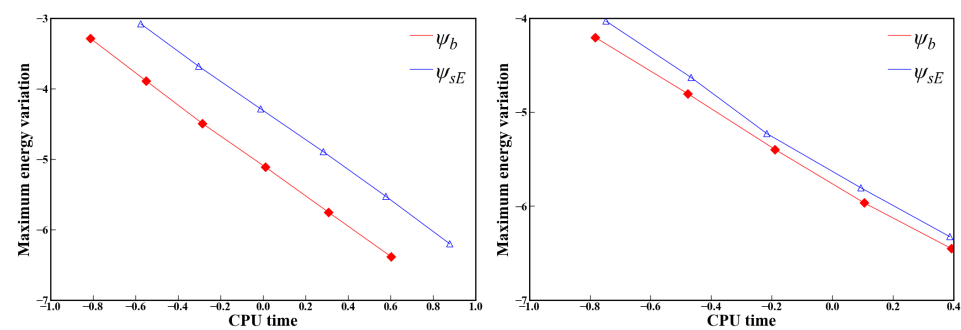


Figure 5. Maximum energy variation $\text{err}_H(\Delta t)$ versus the CPU time in double logarithmic scale, which are given by ψ_b and ψ_{sE} with the initial values of orbit 1 (left) and orbit 2 (right).

5.3. High Order Composition Method

To show the strength of ψ_b , we construct the high order integrators ψ_b^{10} and ψ_{sE}^{10} by composition method, at the same time, we check the work efficiency of ψ_b^{10} by comparing with ψ_{sE}^{10} and the 10th order Gauss Runge–Kutta method ψ_{grk} .

At first, we present the one step integrator of ψ_b [11] with the form of

$$\begin{cases} \mathbf{x}_{n+\frac{1}{2}} = \mathbf{x}_n + \frac{\Delta t}{2} \mathbf{v}_n \\ \frac{\mathbf{v}_{n+1} - \mathbf{v}_n}{\Delta t} = -2\Omega \times \frac{\mathbf{v}_{n+1} + \mathbf{v}_n}{2} - \nabla \varphi(\mathbf{x}_{n+\frac{1}{2}}) \\ \mathbf{x}_{n+1} = \mathbf{x}_{n+\frac{1}{2}} + \frac{\Delta t}{2} \mathbf{v}_{n+1}, \end{cases} \quad (27)$$

and

$$\begin{cases} \mathbf{x}_{n+\frac{1}{2}} = \mathbf{x}_n + \frac{\Delta t}{2} \mathbf{v}_n \\ \mathbf{v}_{n+1} = T(D\mathbf{v}_n - \Delta t \nabla \varphi(\mathbf{x}_{n+\frac{1}{2}})) \\ \mathbf{x}_{n+1} = \mathbf{x}_{n+\frac{1}{2}} + \frac{\Delta t}{2} \mathbf{v}_{n+1}. \end{cases} \quad (28)$$

It is well-known that one can obtain a higher order symmetric integrator by composition of the symmetric integrator. We derive the 10th order explicit, symmetric, symplectic integrator ψ_b^{10} (and ψ_{sE}^{10}) by composition of the explicit, symmetric, symplectic integrator ψ_b (and ψ_{sE}) using the best 35-stage method (Formula (17) in Sofroniou [23]). In addition, one can obtain an arbitrary high order integrator by the composition skills [17].

In our numerical implementation of the implicit Runge–Kutta method ψ_{grk} , we apply fixed point iteration with starting values computed by extrapolation from the previous step. Figure 6 shows that the work efficiency diagram of maximum energy variation along the trajectory versus the CPU times (in seconds) in double logarithmic scale, which are given by ψ_b^{10} , ψ_{sE}^{10} and ψ_{grk} , the initial values are the orbit 1 and orbit 2 in the above numerical experiment 2. We conclude that our integrator ψ_b^{10} is more efficient than ψ_{sE}^{10} and ψ_{grk} .

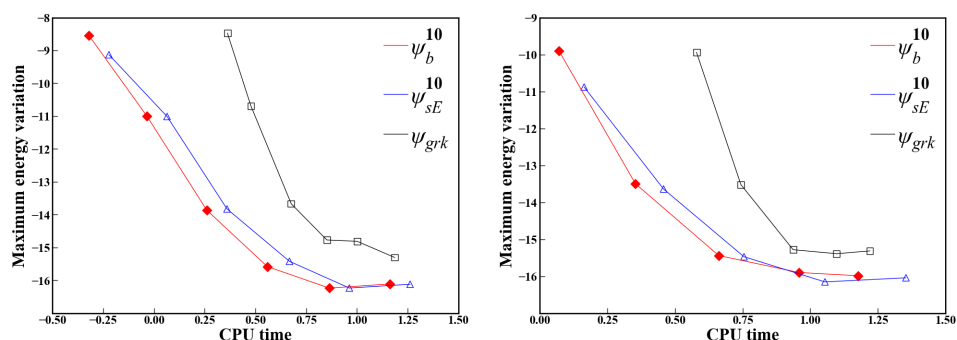


Figure 6. Maximum energy variation $\text{err}_H(\Delta t)$ versus the CPU time in double logarithmic scale, which are given by ψ_b^{10} , ψ_{sE}^{10} and ψ_{grk} , the initial values are orbit 1 (left) and orbit 2 (right) in above numerical experiment 2.

6. Conclusions

In this paper, for the circular restricted three-body problem, we investigated the explicit symmetric numerical integrator ψ_b . In particular, the property of near-conservation of energy for long-term evolution and the symplectic property are derived for the integrator ψ_b . It is important that our 10th order explicit, symmetric, symplectic integrator ψ_b^{10} is more efficient than the 10th order symplectic Euler method ψ_{sE}^{10} and the 10th order implicit Gauss Runge–Kutta method ψ_{grk} for the circular restricted three-body problem.

Two groups of numerical experiments, rotating quadratic potential and earth-moon system, are carried out to verify our theoretical analysis. In addition, the work efficiency comparison of the high order methods presented in Section 5.3 demonstrates the precision, high efficiency, and advantages of easy generation of high order methods of our method.

Author Contributions: Funding acquisition, Q.W. and Y.T.; Investigation, X.T. and Q.W.; Methodology, X.T.; Software, X.T.; Validation, X.T., Q.W. and Y.T.; Writing—original draft, X.T.; Writing—review & editing, Q.W. and Y.T. All authors have read and agreed to the published version of the manuscript.

Funding: This research was funded by National SKA Program of China (Grant No. 2020SKA0110401), National Natural Science Foundation of China (Grant No. 11988101, 12171466).

Institutional Review Board Statement: Not applicable.

Informed Consent Statement: Not applicable.

Data Availability Statement: Not applicable.

Acknowledgments: We acknowledge the support from Special Research Assistant Program of the Chinese Academy of Sciences and K.C.Wong Education Foundation.

Conflicts of Interest: The authors declare no conflict of interest.

References

1. Feng, K. On difference schemes and symplectic geometry. In *Proceedings of 1984 Beijing Symposium on Differential Geometry and Differential Equations*; Feng, K., Ed.; Science Press: Beijing, China, 1985; pp. 42–58.
2. Feng, K. Difference Schemes for Hamiltonian Formalism and Symplectic Geometry. *J. Comput. Math.* **1986**, *4*, 279–289.
3. Forest, E.; Ruth, R.D. Fourth-order symplectic integration. *Phys. D Nonlinear Phenom.* **1990**, *43*, 105–117. [[CrossRef](#)]
4. Channell, P.J.; Scovel, C. Symplectic integration of Hamiltonian systems. *Nonlinearity* **1990**, *3*, 231–259. [[CrossRef](#)]
5. Candy, J.; Rozmus, W. A symplectic integration algorithm for separable Hamiltonian functions. *J. Comput. Phys.* **1991**, *92*, 230–256. [[CrossRef](#)]
6. Huang, L.Y.; Tian, Z.W.; Cai, Y.X. Compact Local Structure-Preserving Algorithms for the Nonlinear Schrödinger Equation with Wave Operator. *Math. Probl. Eng.* **2020**, *2020*, 4345278. [[CrossRef](#)]
7. Kong, L.H.; Chen, M.; Yin, X.I. A novel kind of efficient symplectic scheme for Klein–Gordon–Schrödinger equation. *Appl. Numer. Math.* **2019**, *135*, 481–496. [[CrossRef](#)]
8. Boris, J. Relativistic plasma simulation-optimization of a hybrid code. In *Proceeding of Fourth Conference on Numerical Simulations of Plasmas*; Naval Research Laboratory: Washington, DC, USA, 1970; pp. 3–67.
9. Qin, H.; Zhang, S.X.; Xiao, J.Y.; Liu, J.; Sun, Y.J.; Tang, W.M. Why is Boris algorithm so good? *Phys. Plasmas* **2013**, *20*, 084503. [[CrossRef](#)]
10. Ellison, C.L.; Burby, J.W.; Qin, H. Comment on “Symplectic integration of magnetic systems”: A proof that the Boris algorithm is not variational. *J. Comput. Phys.* **2015**, *301*, 489–493. [[CrossRef](#)]
11. He, Y.; Sun, Y.J.; Liu, J.; Qin, H. Volume-preserving algorithms for charged particle dynamics. *J. Comput. Phys.* **2015**, *281*, 135–147. [[CrossRef](#)]
12. Zhang, R.L.; Liu, J.; Qin, H.; Wang, Y.L.; He, Y.; Sun, Y.J. Volume-preserving algorithm for secular relativistic dynamics of charged particles. *Phys. Plasmas* **2015**, *22*, 044501. [[CrossRef](#)]
13. He, Y.; Sun, Y.J.; Liu, J.; Qin, H. Higher order volume-preserving schemes for charged particle dynamics. *J. Comput. Phys.* **2016**, *305*, 172–184. [[CrossRef](#)]
14. Hairer, E.; Lubich, C. Energy behaviour of the Boris method for charged-particle dynamics. *BIT Numer. Math.* **2018**, *301*, 969–979. [[CrossRef](#)]
15. Broucke, R.A. *Periodic Orbits in the Restricted Three Body Problem with Earth-Moon Masses*; Technical Report; Jet Propulsion Laboratory: Pasadena, CA, USA, 1968.
16. Murray, C.D.; Dermott, S.F. *Solar System Dynamics*; Cambridge University Press: Cambridge, UK, 1999.
17. Hairer, E.; Lubich, C.; Wanner, G. *Geometric Numerical Integration: Structure-Preserving Algorithms for Ordinary Differential Equations*, 2nd ed.; Springer: Berlin, Germany, 2006.
18. Tang, Y.F. Formal energy of a symplectic scheme for hamiltonian systems and its applications (I). *Comput. Math. Appl.* **1994**, *27*, 31–39.
19. Gao, F.B.; Zhang, W. A Study on Periodic Solutions for the Circular Restricted Three-body Problem. *Astron. J.* **2014**, *148*, 116. [[CrossRef](#)]
20. Perdomo, O. On the period of the periodic orbits of the restricted three body problem. *Celest. Mech. Dyn. Astron.* **2017**, *129*, 89–104. [[CrossRef](#)]
21. Abouelmagd, E.I.; Guirao, J.L.G.; Pal, A.K. Periodic solution of the nonlinear Sitnikov restricted three-body problem. *New Astron.* **2020**, *75*, 101319. [[CrossRef](#)]
22. Tu, X.B.; Murua, A.; Tang, Y.F. New high order symplectic integrators via generating functions with its application in many-body problem. *BIT Numer. Math.* **2020**, *129*, 509–535. [[CrossRef](#)]
23. Sofroniou, M.; Spaletta, G. Derivation of symmetric composition constants for symmetric integrators. *Optim. Methods Softw.* **2005**, *20*, 597–613. [[CrossRef](#)]